ACSNANO

www.acsnano.org

ARTICLE

Binary Colloidal Crystals Promote Cardiac Differentiation of Human Pluripotent Stem Cells via Nuclear Accumulation of SETDB1

Yongping Lin,[#] Feng Zhang,[#] Shaojie Chen,[#] Xiyu Zhu, Jincheng Jiao, Yike Zhang, Zhaomin Li, Jiao Lin, Biao Ma, Minglong Chen,[*] Peng-Yuan Wang,[*] and Chang Cui[*]

Cite This: *ACS Nano* 2023, 17, 3181−3193

Read Online

ACCESS | Metrics & More | Article Recommendations | Supporting Information

ABSTRACT: **Biophysical cues can facilitate the cardiac differentiation of human pluripotent stem cells (hPSCs), yet the mechanism is far from established. One of the binary colloidal crystals, composed of 5 μm Si and 400 nm poly(methyl methacrylate) particles named 5PM, has been applied as a substrate for hPSCs cultivation and cardiac differentiation. In this study, cell nucleus, cytoskeleton, and epigenetic states of human induced pluripotent stem cells on the 5PM were analyzed using atomic force microscopy, molecular biology assays, and the assay for transposase-accessible chromatin sequencing (ATAC-seq). Cells were more spherical with stiffer cell nuclei on the 5PM compared to the flat control. ATAC-seq revealed that chromatin accessibility decreased on the 5PM, caused by the increased entry of histone lysine methyltransferase SETDB1 into the cell nuclei and the amplified level of histone H3K9me3 modification. Reducing cytoskeleton tension using a ROCK inhibitor attenuated the nuclear accumulation of SETDB1 on the 5PM, indicating that the effect is cytoskeleton-dependent. In addition, the knockdown of SETDB1 reversed the promotive effects of the 5PM on cardiac differentiation, demonstrating that biophysical cue-induced cytoskeletal tension, cell nucleus deformation, and then SETDB1 accumulation are critical outside-in signal transformations in cardiac differentiation. Human embryonic stem cells showed similar results, indicating that the biophysical impact of the 5PM surfaces on cardiac differentiation could be universal. These findings contribute to our understanding of material-assistant hPSC differentiation, which benefits materiobiology and stem cell bioengineering.**

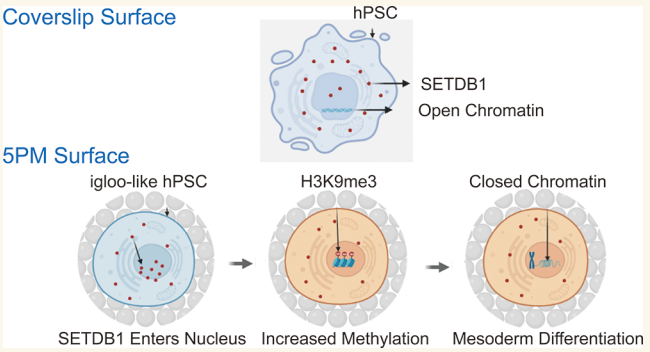

KEYWORDS: *biophysical cues, topography, pluripotent stem cell, epigenetics, histone modulation*

INTRODUCTION

Human pluripotent stem cell (hPSC)-derived cardiomyocytes (CMs) are a promising cell source for transplantation, drug screening, and organ-on-chip platforms.[1] The stem cell niche *in vivo* is varying combinations of biochemical and biophysical cues in a wide range. Since the discovery of hPSCs, many studies have focused on regulating hPSC differentiation using biochemical factors.[2] Previous studies demonstrated that materials with a soft mechanical property or a specific surface structure could also facilitate stem cell differentiation, shedding light on modulating stem cell decision-making using biophysical cues.[3,4] Indeed, developing an optimized bioengineering approach for cardiac differentiation of hPSCs *in vitro* will be highly beneficial for cardiac regenerative medicine.

Epigenetic regulation is critical in cardiac development. It has been recently reported that cell nuclei of CM integrated mechanical cues from the environment through the reorganization of epigenetically marked chromatin, thereby stabilizing differentiation and a mature phenotype.[5] When planted on a dendrimer-immobilized surface, human mesenchymal stem cells (hMSCs) reorganized the nuclear lamina and cytoskeleton and remodeled the histone modifications, consequently shifting the cells from the multipotent state to the smooth, skeletal, and cardiac muscle lineages.[6] Steven's group has demonstrated that parallel microgrooves enhanced the directed

Received: January 1, 2023
Accepted: January 17, 2023
Published: January 19, 2023

https://doi.org/10.1021/acsnano.3c00009
ACS Nano 2023, 17, 3181−3193

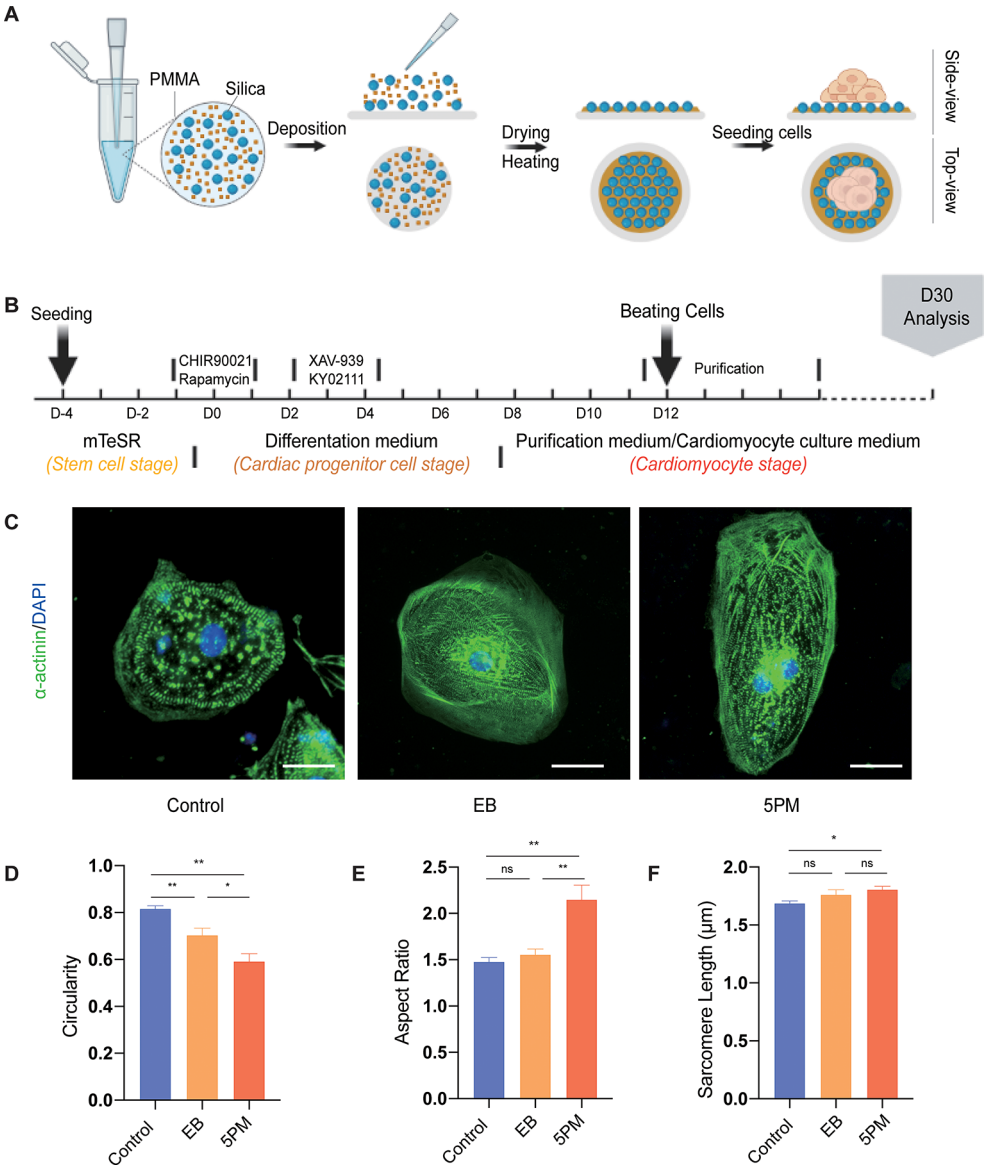

Figure 1. 5PM prompted the cardiac differentiation. (A) Manufacturing of the BCCs substrate. (B) Flowchart of cardiac differentiation of hiPSCs on control and 5PM surfaces. (C) Immunostaining of hiPSC-CMs derived from control, 5PM surface, and EB formation (nucleus: blue, α-actinin: green, scale bars = 50 μm). The circularity (D), aspect ratio (E), and sarcomere length (F) of hiPSC-CMs in the three groups were statistically analyzed (n = 30). Mean ± SEM is shown. *p < 0.05, **p < 0.01, ***p < 0.001, estimated by one-way ANOVA with Tukey's test.

differentiation of cardiac progenitors into CM-like cells. Such biophysical effects inhibited the activity of histone deacetylase, augmenting the expression of CM-specific proteins in the genetically engineered cells.[7] These findings highlighted the epigenetic modification in response to mechanical stimuli during cardiogenesis.

Our group developed a family of nanostructured substrates called colloidal self-assembled patterns (cSAPs) for stem cell differentiation.[8] One of the cSAPs named binary colloidal crystals (BCCs), composed of two types of particles, have been applied to stem cell culture.[8,9] Particle size, material, proportion, and surface functional groups can be tuned prior to self-assembly; hence, rich surface physicochemical signals can be designed for tuning cellular function. Recently, we demonstrated that one of the BCCs, composed of 5 μm silica particles and 400 nm poly(methyl methacrylate) (PMMA) particles (named 5PM) could promote CM differentiation of hiPSCs, but the underlying mechanism is unclear.[8]

In the present study, we aimed to discover the mechanism of BCC-mediated hPSC differentiation. We noticed that cell morphology was dramatically distinct between 5PM surface and the flat control, which lead to a better cardiac differentiation on the 5PM. Thus, it is hypothesized that focal adhesions, cell nucleus, and cytoskeleton are vital modulators in hiPSC differentiation. Herein, we examined the epigenetic state of hiPSCs using the assay for transposase accessible chromatin sequencing (ATAC-seq) and verified whether the biophysical effect of the BCC is universal using hiPSCs and hESCs. This study explored the mechanism of BCC-mediated cardiac differentiation, which provides insights into mechanotransduction and benefits stem cell bioengineering.

https://doi.org/10.1021/acsnano.3c00009
ACS Nano 2023, 17, 3181−3193

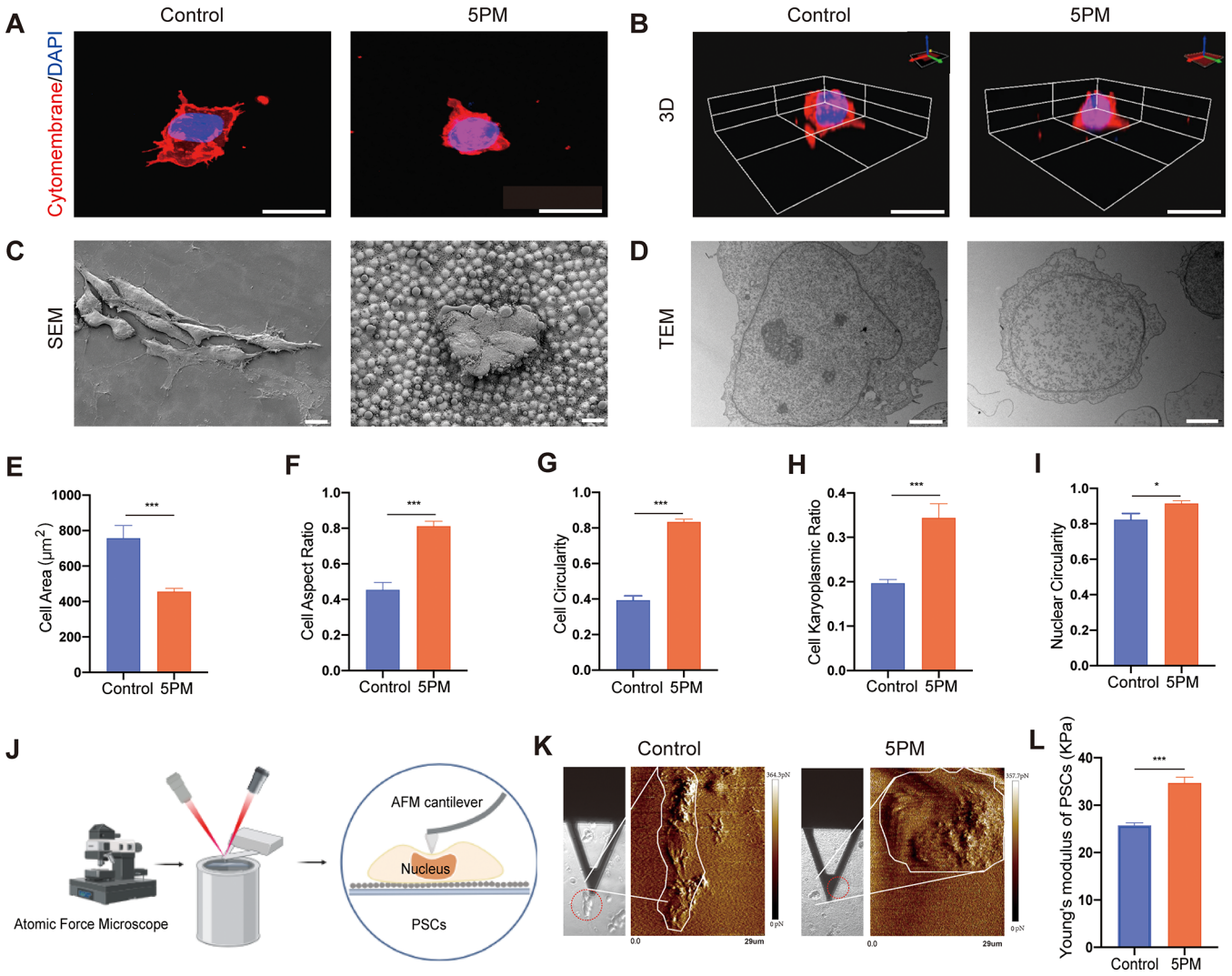

Figure 2. Morphological and mechanical characterization of cells. (A) Fluorescence staining images of cytomembrane (Dil, red) and nuclei (DAPI, blue) in hiPSCs cultured on 5PM and control coverslips (scale bars = 20 μm). (B) 3D-reconstructed images of the basal surface of stained hiPSCs (scale bars = 20 μm). (C) Scanning electron microscopy (SEM) images of hiPSC colonies on 5PM and control coverslips (scale bars = 10 μm). (D) Transmission electron microscopy (TEM) scan of microstructures in hiPSCs on 5PM and control coverslips (scale bars = 2 μm). Based on the fluorescence staining, the cell area (E), cell aspect ratio (F), cell circularity (G), and cell karyoplasmic ratio (H) in the two groups were statistically analyzed (n = 15−19). (I) The circularity of the hiPSCs nuclei in the two groups was analyzed based on the TEM scan (n = 9). (J) AFM diagram of hiPSCs. (K) Morphology of hiPSCs on control and 5PM surface by AFM scan. The left panel displayed the probe and hiPSCs (red circle) in the bright field. (L) Young's modulus analysis of hiPSCs on control and 5PM surface (n = 10). Mean ± SEM is shown. *p < 0.05, **p < 0.01, ***p < 0.001, estimated by two-sample t test.

RESULTS AND DISCUSSION

BCCs Prompted the Cardiac Differentiation of hiPSCs. When interacting with materials, adhered cells are stimulated by various physicochemical signals, including topographical cues, heat, electricity, and magnetism. Among these physical signals, the regulatory effect of substrate physicochemical signals on hPSCs is of most interest to researchers because it is a one-step method that is feasible in most laboratories.[10,11] Various projects have illuminated the promoting effects of surface topographical cues such as micro/nanogroove,[7,12] pillar,[13] and hierarchical patterns[14] on cardiac differentiation and maturation of hPSCs.

BCCs are versatile materials with hierarchical surface structures and heterogeneous surface chemistries[15] that can be fabricated in a short period (Figure 1A). We previously revealed that BCC composed of 5 μm Si and 400 nm PMMA particles, named 5PM, with hexagonal close-packed geometry can improve the all-around maturation of hiPSC-CMs, including mature structural and electrophysiological properties.[8]

hiPSCs on 5PM substrates formed igloo-like colonies and 3D spheroids depending on the size which is similar to attached embryoid bodies (EBs).[8] To show the effect of 5PM surface, the surface characteristics of 5PM were analyzed using X-ray photoelectron spectroscopy (XPS), atomic force microscope (AFM), and scanning electron microscopy (SEM) (Figure S1). Meanwhile, the sarcomere structures of the reseeded hiPSC-CMs cultured on the control coverslip, 5PM surface, and via EB formation were compared as a single cell analysis. Before that, teratoma and karyotype assays were conducted to prove the good quality of the hiPSCs (Figure S2). As the immunofluorescence staining showed, the 5PM-derived hiPSC-CMs (Figure 1B) exhibited significantly lower

https://doi.org/10.1021/acsnano.3c00009
ACS Nano 2023, 17, 3181−3193

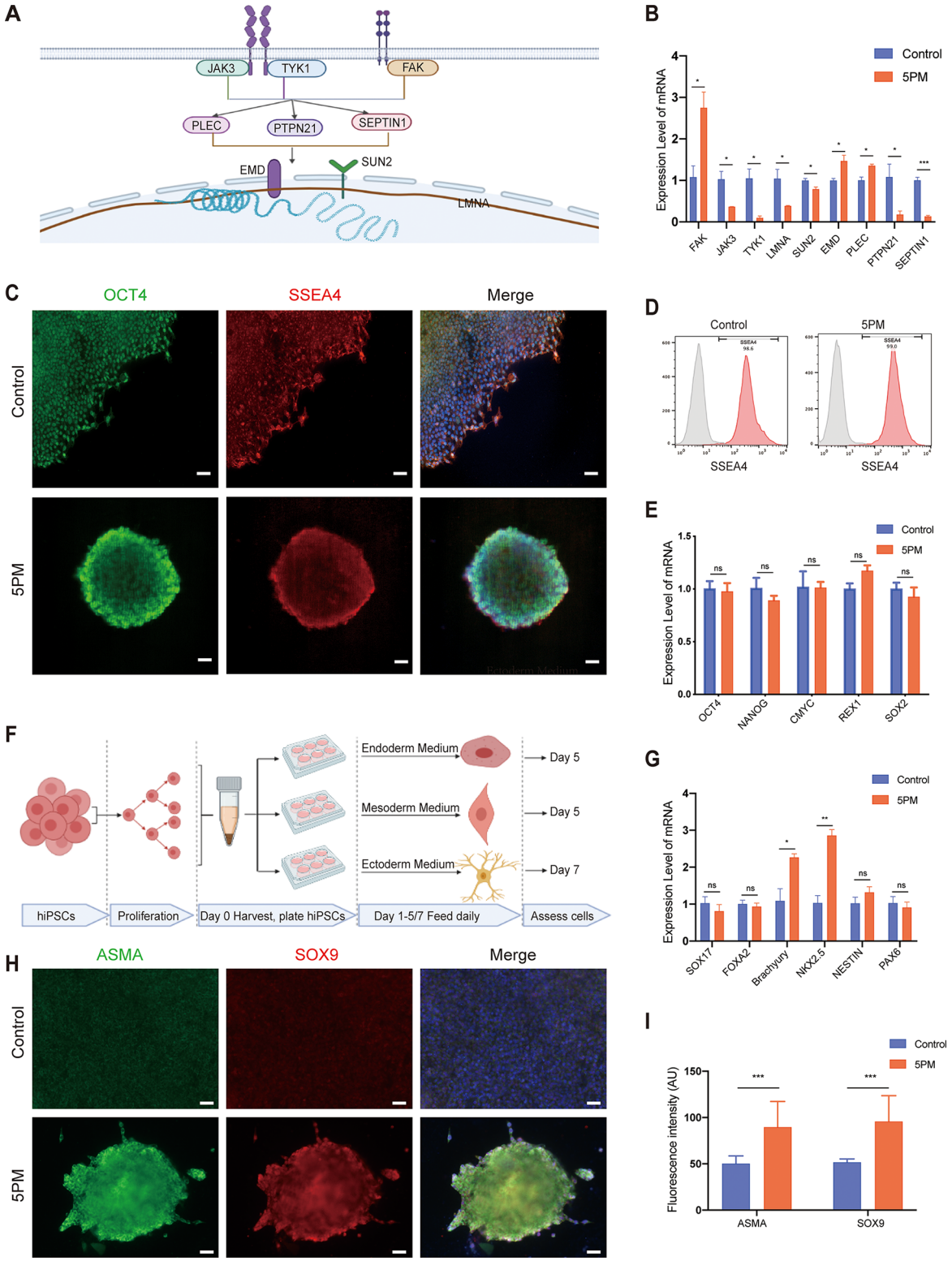

Figure 3. Pluripotency analysis of hiPSCs on different surfaces. (A) Distribution of cellular adhesion, LINC complex, and cytoskeleton related proteins, including FAK, JAK3, TYK1, LMNA, SUN2, EMD, PLEC, PTPN21, and SEPTIN in cells. (B) The expressions of genes mentioned above were analyzed by *qRT-PCR* (n = 3). (C) Immunostaining of pluripotent markers in hiPSCs from control and 5PM group (nucleus: blue, OCT4: green, SSEA4: red, scale bars = 100 μm). (D) Flow cytometry analysis of pluripotent markers, SSEA4, in hiPSCs cultured on 5PM and control coverslips. (E) The expression levels of stemness related genes, including OCT4, NANOG, CMYC, REX1, SOX2 were analyzed by *qRT-PCR* (n = 3). (F) Schematic diagram of hiPSCs trilineage differentiation induced with Trilineage Differentiation Kit. (G) Trilineage differentiation capacity was characterized via *qRT-PCR* (endoderm: SOX17, FOXA2, mesoderm: Brachyury, NKX2.5, ectoderm: NESTIN, PAX6, respectively). n = 3. (H) Immunostaining of mesoderm markers (ASMA, SOX9) in hiPSCs from control and 5PM group, after the induction of mesoderm differentiation (scale bars = 100 μm). (I) The fluorescence intensity of each mesoderm marker was further compared (n = 9). Mean ± SEM is shown. *p < 0.05, **p < 0.01, ***p < 0.001, estimated by two-sample t test.

https://doi.org/10.1021/acsnano.3c00009
ACS Nano 2023, 17, 3181−3193

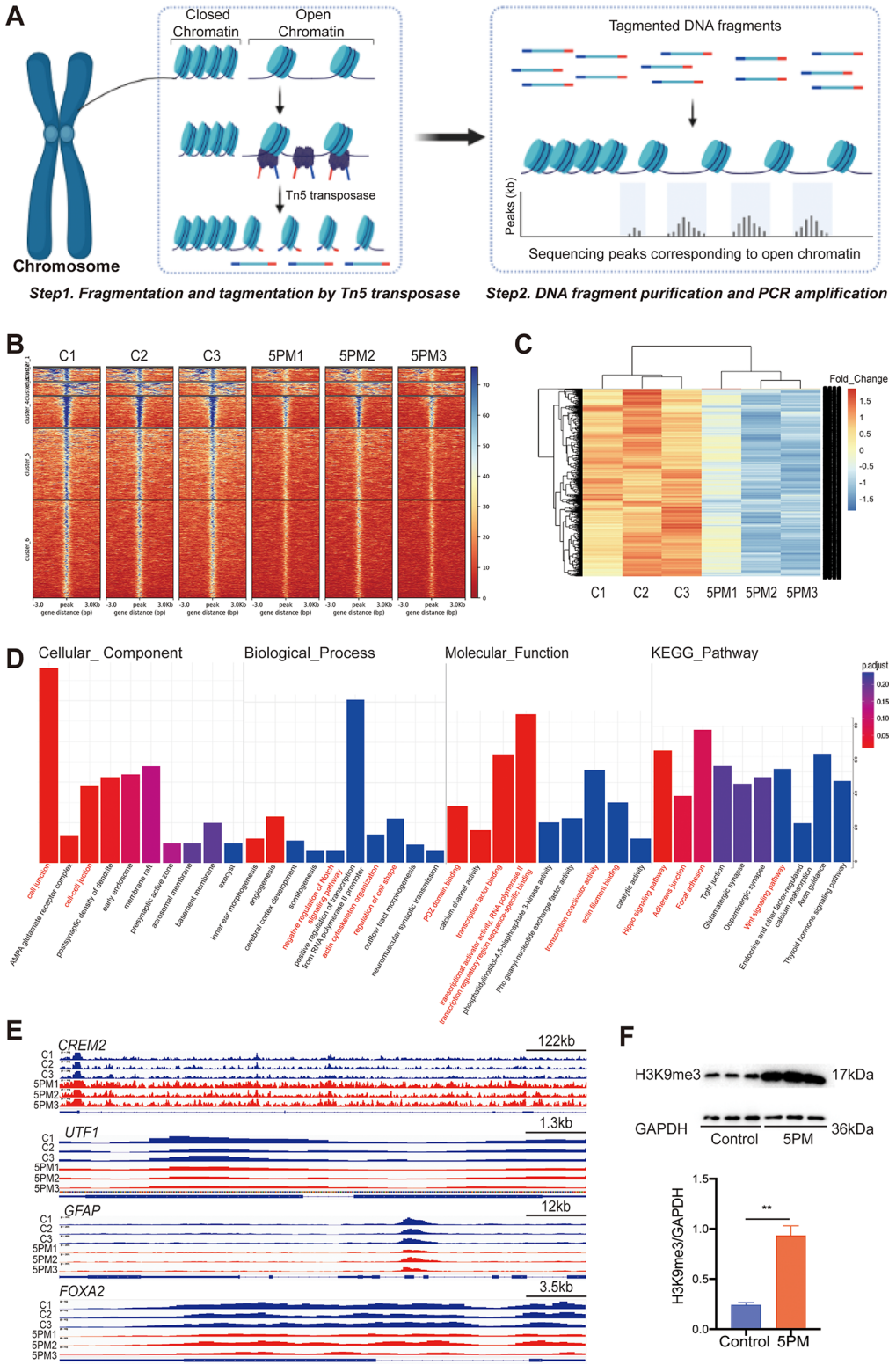

Figure 4. Chromatin accessibility analysis of hiPSCs cultured on different surfaces. (A) Schematic diagram of ATAC-seq. (B) Heatmaps show accessibility around differential peaks in each group of samples. The *X*-axis represents the position of 3KB upstream and downstream with peak as the center, where −3KB represents 3KB upstream of peak center and 3KB represents 3KB downstream of peak center. The *Y*-axis represents the signal value enriched by reads. The larger the value, the more enriched it is. (C) Heatmaps of differential expressed genes forecast according to their corresponding peak numbers in each group of all samples. (D) GO enrichment map and KEGG pathway enrichment map of associated genes in differential peak region. (E) The representative genome tracks of ATAC-Seq reads in hiPSCs cultured on 5PM and control surfaces were exhibited, including CREM2, UTF1 (regulators involved in mesoderm development), GFAP (ectoderm marker), FOXA2 (regulators involved in endoderm development). Blue: control group, Red: 5PM group. (F) The content of H3K9me3 levels in hiPSCs on 5PM and control coverslips was detected by Western Blot ($n = 3$). Mean ± SEM is shown. *$p < 0.05$, **$p < 0.01$, ***$p < 0.001$, estimated by two-sample *t* test.

https://doi.org/10.1021/acsnano.3c00009
ACS Nano 2023, 17, 3181−3193

circularity, higher aspect ratio, and longer sarcomere length, compared to the age-matched controls and EB-CMs (Figure S3), indicating an inferior level of cardiac maturation[16] (Figure 1C−F).

Cardiac differentiation of hPSCs on the 5PM surface is a one-stop method for CM generation *in situ*, which would be highly beneficial for robust CM production. Nevertheless, the concrete mechanism of the 5PM promoting cardiac differentiation is unclear. An in-depth exploration of this subject will advance our understanding of how biophysical cues influence cell behavior.

BCCs Prompted Nuclear Stiffness of hiPSCs. Cell morphology of hiPSCs on 5PM surface was analyzed using a confocal microscope, TEM, and SEM (Figure 2A−D). The hiPSCs on the 5PM surface had distinct cell and nucleus shapes, compared with the flat control. Single hiPSC cultured on the 5PM surface showed a smaller cell size and denser cytoplasm compared to the control (Figure 2A). The 3D-reconstructive morphology of the cells further showed that the single hiPSC on 5PM surface had a more spherical shape (Figure 2B). hiPSCs on 5PM surface had significantly smaller cell size (∼0.6-fold, Figure 2E), higher aspect ratio (∼2-fold, Figure 2F), higher circularity (∼2.0-fold, Figure 2G), and higher cell karyoplasmic ratio (∼1.7-fold, Figure 2H) compared to the control. Dense and round hiPSC clusters were observed on the 5PM surface, while loose and irregular hiPSC colonies were found on the control coverslip (Figure 2C). The shape of the cell nucleus was examined using TEM images (Figure 2D). Cell nuclei of hiPSCs cultured on 5PM surface showed significantly increased nuclear roundness compared with controls (∼1.1-fold, Figure 2I). The AFM test demonstrated that Young's modulus of cell nuclei on the 5PM surface was significantly higher than that on the control coverslips (∼1.4-fold, Figure 2J−L). The mechanical properties of the cell nucleus, such as stiffness, are essential in regulating various physiological and pathological processes, including cell differentiation, migration, adhesion, and metastasis. Hence, we speculated that 5PM surface could remodel the properties of hiPSCs even before the induction of cardiac differentiation.

BCCs Remodeled Cellular Structures and Prompted Mesoderm Differentiation of hiPSCs. Cell adhesion determines the spatial reorganization of the cytoskeleton and cell morphology.[17] Apical actin stress fibers are directly connected to the nuclear lamina through the linker of nucleoskeleton and cytoskeleton (LINC) complexes, which are essential to maintain nuclear shape and regulating chromosome dynamics. Mechanotransduction is the mechanism by which cells convert mechanical stimuli from the extracellular microenvironment into intracellular biophysical signals to induce various cellular responses. It is becoming clear that the mechanotransduction process involves distinct cytoskeletal and LINC complex components. Herein, we tested the gene expressions coding for integrins (seven ITGA and eight ITGB subtypes), cell adhesion (FAK, JAK3, and TYK1), LINC complex (LMNA, SUN2, and EMD), and cytoskeleton (PLEC, PTPN21, and SEPTIN1) in hiPSCs cultured on BCCs (Figure 3A). The result showed a dramatic difference in the expression profiles of these structural genes between the two groups (Figure 3B). There were no significant differences in the expressions of integrin subtypes in hiPSCs cultured between 5PM and flat control, although ITGA10 was slightly higher and ITGB2/3 were slightly lower on 5PM (Figure S4).

Pluripotency is defined by the expression of pluripotent markers (e.g., OCT4, NANOG, SOX2, and SSEA4) and the ability to differentiate into three lineages (i.e., endoderm, mesoderm, and ectoderm).[18] The pluripotent markers, i.e., OCT4 and SSEA4, showed similar protein expression levels in hiPSCs cultured on the 5PM and control surfaces tested by immunostaining and FACS analysis (∼99%, Figure 3C,D). Similarly, the mRNA expression levels of pluripotent markers, including OCT4, NANOG, CMYC, REX1, and SOX2 in hiPSCs showed no differences between the two groups (Figure 3E).

On the other hand, hiPSCs were cultured on 5PM and control surfaces without chemical factors for cardiac differentiation. It is consistent with the pluripotent staining in Figure 3C that the immunostaining of cardiac markers was negative in both groups (Figure S5). Subsequently, we induced trilineage differentiation in hiPSCs cultured on 5PM and control coverslips using commercial kits (Figure 3F). Interestingly, two mesoderm genes, Brachyury and NKX2.5, key transcription factors for cardiac differentiation, were significantly enhanced in the 5PM group (Figure 3G). However, the expressions of endoderm or ectoderm genes showed no differences between the two groups. Brachyury and its coexpressed CDX2 mediated BMP-induced differentiation of human and mouse pluripotent stem cells into mesoderm and inhibited endoderm differentiation.[19] NKX2.5 is essential in the mesoderm for early heart formation.[20] Furthermore, the immunofluorescence stainings of mesoderm markers (ASMA, SOX9), endoderm markers (FOXA2, SOX17), and ectoderm markers (TUJ1, GFAP) were analyzed as reported before.[21] In parallel, the 5PM surface prompted mesoderm differentiation of hiPSCs (Figure 3H,I). However, there were no differences in endoderm and ectoderm markers in the induced hiPSCs (Figure S6). This is consistent with the previous findings that the process of differentiation from pluripotent cells to functional end-phenotypes is mechanoresponsive in a lineage- and differentiation stage-specific manner.[22]

BCCs Decreased the Chromatin Accessibility of hiPSCs. hiPSCs have been reported to have less condensed chromatin, as they are capable of differentiating into any cell type. The differentiation of hiPSCs is accompanied by a selective condensation into heterochromatin with concomitant gene silencing, leaving access only to lineage-specific genes in the euchromatin.[23] Mechanical and physical forces can alter nuclear shape and mechanics via heterochromatin formation.[24] Thus, we evaluated the epigenetic status and chromatin accessibility using ATAC-seq (Figure 4A, Figure S7, and Table S1).

As shown in Figure 4B, hiPSCs cultured on 5PM surfaces exhibited decreased chromatin accessibility, compared with the control group. According to their corresponding peak numbers, the forecasted gene expression of 5PM group was significantly downregulated compared with that in the control group (Figure 4C). Further Gene Ontology (GO) and Kyoto Encyclopedia of Genes and Genomes (KEGG) analysis of differentially expressed genes in the forecast indicated strong enrichment for genes involved in cardiogenesis (i.e., Wnt, Notch, and Hippo[25−27]), cellular structure (i.e., cell junction, focal adhesion, actin cytoskeleton organization, actin filament binding), and transcriptional regulation (i.e., transcription factor binding, transcription coactivator activity, PDZ domain

https://doi.org/10.1021/acsnano.3c00009
ACS Nano 2023, 17, 3181−3193

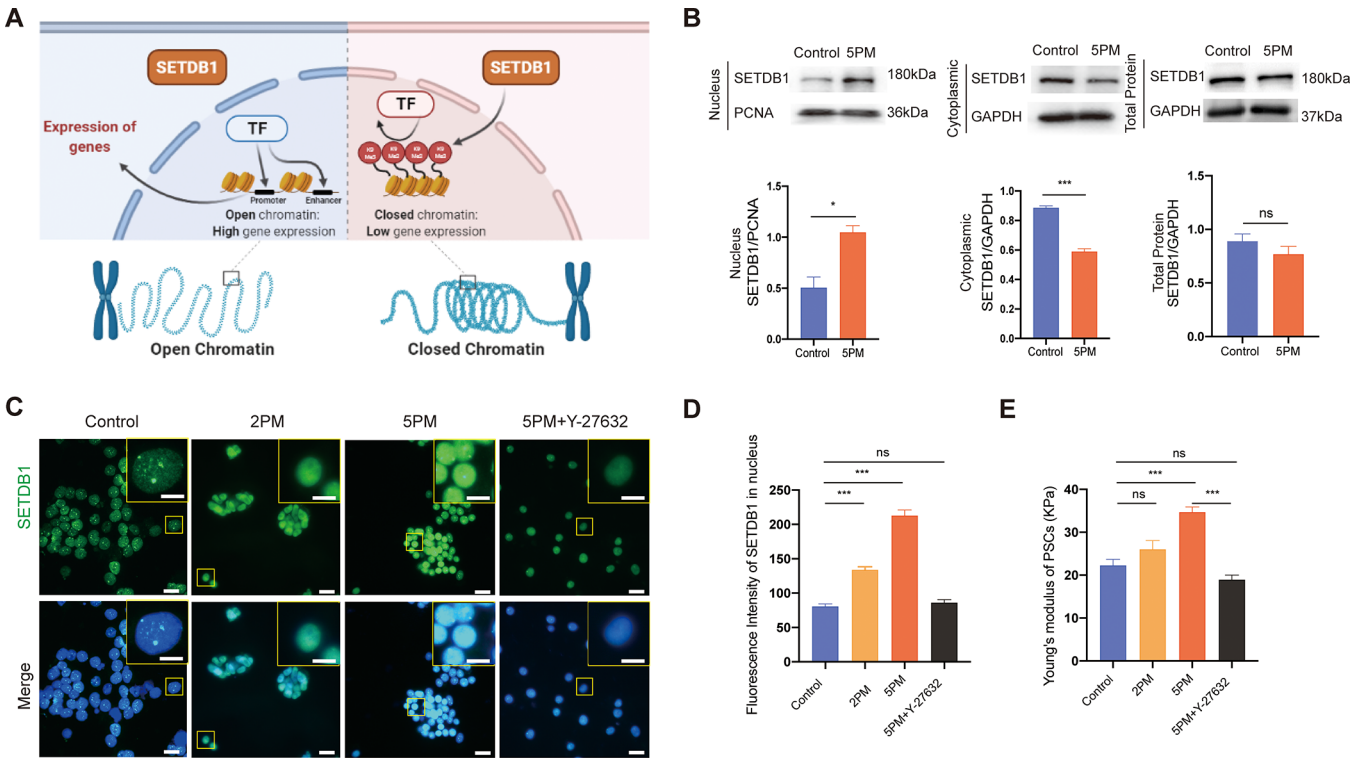

Figure 5. 5PM prompted the nuclear transfer of SETDB1 in hiPSCs. (A) Schematic diagram of SETDB1 function, which regulates transcriptional repression by histone methylation. (B) The total, cytoplasmic, and nuclear protein expressions of SETDB1 were analyzed by Western Blot in hiPSCs grown on 5PM and control coverslips (n = 3). (C) Immunofluorescence staining was used to observe the nuclear distribution of SETDB1 in the control, 2PM, 5PM, and 5PM treated with Y-27632 group (nucleus: blue, SETDB1: green, scale bars = 20 μm, zoomed scale bars = 10 μm). (D) The fluorescence intensity of SETDB1 inside the nuclei in each group was statistically analyzed by ImageJ (n = 10). (E) The nuclear stiffness of hiPSCs cultured on control coverslip, 2PM, 5PM, and 5PM with Y-27632 treatment was analyzed by AFM (n = 10). Mean ± SEM is shown. *p < 0.05, **p < 0.01, ***p < 0.001, B was estimated by two-sample t test, D and E were estimated by one-way ANOVA with Tukey's test.

binding, transcription regulatory region sequence-specific binding) (Figure 4D and Table S2). On the other side, the representative genome tracks of ATAC-seq reads in hiPSCs cultured on 5PM and control surfaces were exhibited in Figure 4E. The large-scale chromatin opening of GREM2[28] and chromatin closing of UTF1[29] in hiPSCs from the 5PM group may allow the expressions of transcriptional regulators of cardiogenesis. Yet, the remodeling of chromatin accessibility on the 5PM surface was not favorable for the endoderm and ectoderm differentiation (Figure S8).[30]

Generally, gene silencing could be performed by trimethyl histone H3 on lysine 9 and 27 (H3K9 and H3K27), and gene activation could be regulated by trimethylation of histone H3 at lysine 4 (H3K4), by influencing chromatin accessibility.[31] We further compared the histone methylation state between the two groups. In the detection of the methylation of H3K4, H3K9, and H3K27, the expression level of H3K9me3 was significantly increased in the 5PM group (Figure 4F), while H3K4me3 and H3K27me3 proteins showed no differences between the two groups. Meanwhile, the expression level of H3K9me2 was also elevated in the 5PM group (Figure S9).

BCCs Increased the Nuclear Transport of SETDB1 in hiPSCs. The lysine methyltransferase, SETDB1, is one of the enzymes responsible for modulating the methylation of H3K9 and plays a role in diverse biological processes, including early development, immune cell development, and muscle differentiation.[32] Multiple mechanisms could induce the nuclear transport and accumulation of SETDB1, mediating the silence of genes and retrotransposons with H3K9me3 modification (Figure 5A).[33] Therefore, we compared the total, nuclear, and cytoplasmic protein levels of SETDB1 in hiPSCs cultured on the 5PM and control coverslip. The cytoplasmic SETDB1 protein was significantly decreased, while the nuclear SETDB1 was significantly increased in the 5PM group. Meanwhile, the total protein levels of SETDB1 showed no differences between the 5PM and control groups, indicating the relocation of SETDB1 from the cytoplasm to the cell nucleus (Figure 5B).

On the other hand, Y-27632 is a selective Rho-associated coiled coil-forming kinase (ROCK) inhibitor causing downstream inhibition of myosin II phosphorylation, reported to reduce the cytoskeleton tension of cancer-associated fibroblasts[34] and mouse embryonic stem cells.[35] To validate whether the relocalization of SETDB1 was driven by biophysical cues from the 5PM surface, we thus added Y-27632 to soften the cells. Moreover, the 2PM group was set as a topographical control. Due to the low-attached characteristics of hiPSCs, BCC substrates and control surfaces were all coated with Matrigel to improve the adhesion. We initially compared the surface stiffness of BCCs and control coverslips with and without the Matrigel coating. As shown in Figure S10, the 5PM surface in the presence of Matrigel coating exhibited a slightly lower Young's modulus compared with the plain 5PM, but without statistical differences. Nevertheless, the stiffness of 5PM+Matrigel was higher than 2PM+Matrigel (~1.8 fold) and control coverslip+Matrigel (~2.1 fold), which showed the same trend as the stiffness of the surfaces alone.

https://doi.org/10.1021/acsnano.3c00009
ACS Nano 2023, 17, 3181−3193

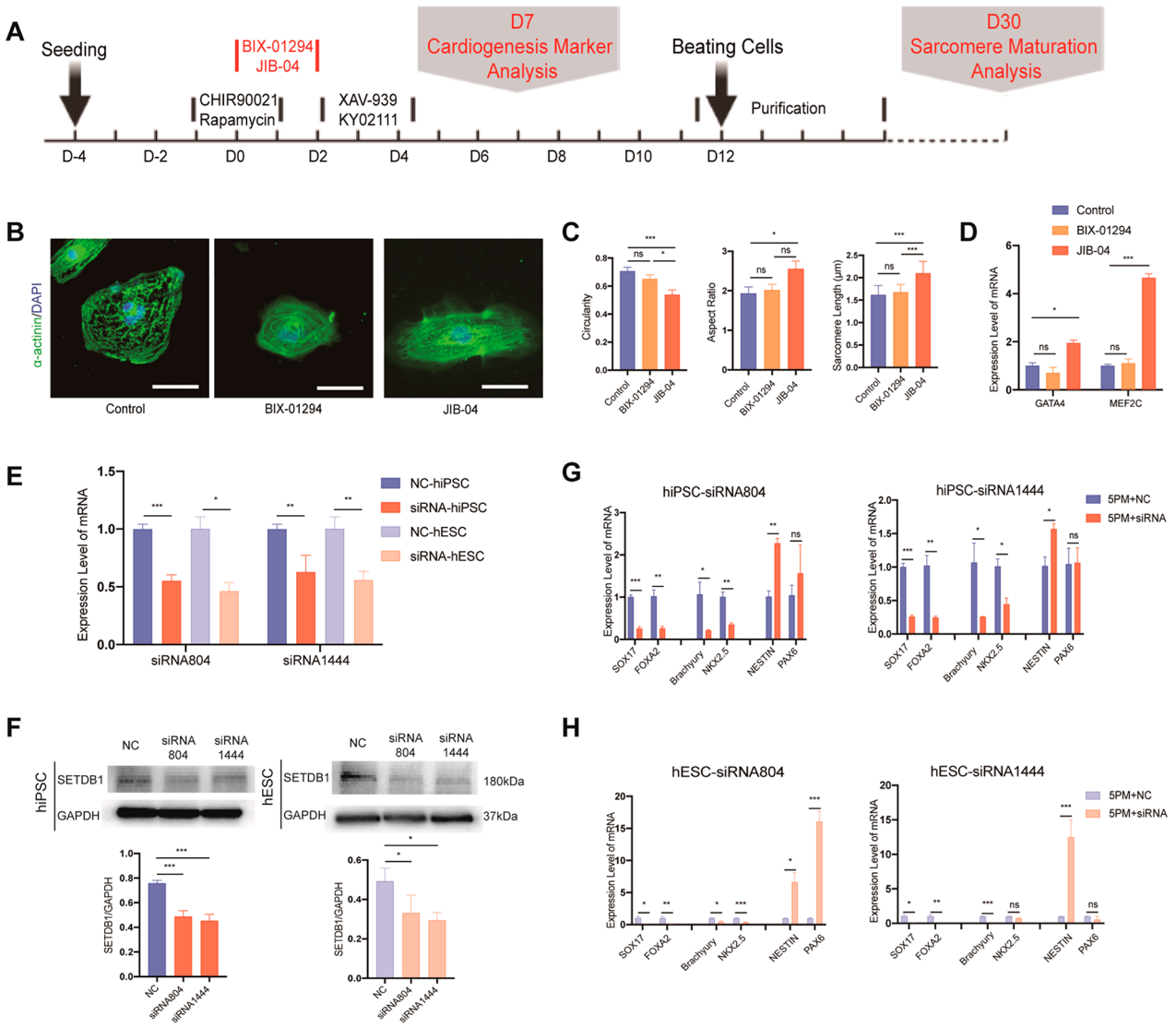

Figure 6. Potent effect on mesoderm differentiation of 5PM surface was reversed by SETDB1 knockdown. (A) Flowchart of modulating SETDB1 activity during cardiac differentiation of hiPSCs. (B) Immunostaining of D30 hiPSC-CMs in the presence of BIX-01294 (a histone methyltransferase inhibitor), JIB-04 (a histone demethylase inhibitor), and blank control (nucleus: blue, α-actinin: green, scale bars = 50 μm). (C) The circularity, aspect ratio, and sarcomere length of hiPSC-CMs in the three groups were statistically analyzed (n = 30). (D) The expression levels of cardiogenesis related genes including GATA4 and MEF2C were analyzed by *qRT-PCR* on D7 (n = 3). (E) Knockdown of SETDB1 with small interfering RNAs (siRNAs) in one hiPSC and one hESC cell lines. Gene expression was determined via *qRT-PCR*. (F) The protein expression level of SETDB1 was detected by Western Blot in two hPSC lines to estimate the interfering efficiency of siRNA-SETDB1 (n = 3), estimated by one-way ANOVA with Dunnett's test. (G,H) Trilineage differentiation capacity was evaluated using *qRT-PCR* analysis after siRNA-SETDB1 treatment in hiPSCs and hESCs on 5PM surface, respectively (n = 3). Mean ± SEM is shown. *p < 0.05, **p < 0.01, ***p < 0.001, C and D were estimated by one-way ANOVA with Tukey's test, E, G, and H were estimated by two-sample t test.

Afterward, the nuclear stiffness and SETDB1 nuclear localization of hiPSCs were evaluated among the control, 2PM, 5PM, and 5PM+Y-27632 groups (Figure 5C). In parallel, AFM analysis demonstrated that Young's modulus of cell nuclei on the 5PM was the highest, followed by the 2PM group and control group. Consistently, the immunofluorescence staining exhibited a notable accumulation of nuclear SETDB1 in the hiPSCs cultured on the 5PM surface, 2PM group was in the middle, and the control group was the lowest (Figure 5D). After treatment of Y-27632, hiPSCs cultured on the 5PM surfaces lost the spherical morphologies (Figure S11) and exhibited soft cell nuclei (Figure 5E). Ultimately, the phenotype of nuclear translocation of SETDB1 was reversed.

The change in nuclear morphology can alter the level of a variety of substances in and out of the nucleus, resulting in epigenetic remodeling. For example, mechanical stretch deforms the nucleus, which cells initially counteract via a calcium-dependent nuclear softening driven by a loss of H3K9me3-marked heterochromatin.[36] Recently, the nuclear transport of DNA methyltransferase 3-like (DNMT3L) is recognized to be promoted by stiff ECM in a protein kinase Cα (PKCα)-dependent manner, leading to gene silencing by condensed chromatin of promoters of pluripotent genes (NANOG), and controls the pluripotency and differentiation of mESCs.[37] These investigations, together with ours, establish a connection between biophysical signals and intracellular epigenetic modifications.

https://doi.org/10.1021/acsnano.3c00009
ACS Nano 2023, 17, 3181−3193

Knockdown of SETDB1 Attenuated the Biophysical Cues of BCCs. It has been demonstrated that SETDB1 restricted extraembryonic trophoblast lineage potential in hPSCs.[38,39] Moreover, H3K9me3-marked heterochromatin controls genome stability and three-trilineage differentiation via distinct epigenomic landscapes. A recent study has revealed that H3K9me3 marked more gene bodies, promoters, and termination transcription sites in endoderm and mesoderm cells when comparing H3K9me3 profiles across the three germ layers.[40] To further support that SETDB1 is vital in cardiac differentiation, we mimicked and reduced the effect of SETDB1 on the early days of cardiogenesis with small molecules, i.e., JIB-04 and BIX-01294, respectively[41] (Figure 6A). It illuminated that JIB-04 (a histone demethylase inhibitor) prompted the sarcomere maturation (Figure 6B,C) and the expressions of cardiogenesis markers (Figure 6D), while BIX-01294 (a histone methyltransferase inhibitor) exhibited opposite phenotypes.

Moreover, human embryonic stem cells (hESC) were another important source for hPSCs. As the immunostaining of cardiac contractile protein (α-actinin) showed, the 5PM surface was also effective to facilitate cardiac differentiation of hESCs (Figure S12). In order to verify whether the 5PM surface affected a variety of hPSCs differentiation by increasing nuclear SETDB1, we used siRNA-SETDB1 (Table S3) to knock down SETDB1 expression in hiPSCs and hESCs. Both siRNAs804 and siRNAs1444 could efficiently reduce the mRNA and protein levels of SETDB1 (Figure 6E,F). Afterward, hiPSCs were differentiated into three germ layers using the Trilineage Differentiation Kit. Knockdown of SETDB1 decreased the expressions of mesoderm markers (i.e., Brachyury and NKX2.5) on the 5PM surface. Furthermore, the expressions of endoderm and ectoderm markers were also changed, where SOX17 and FOXA2 (endoderm) was downregulated and NESTIN and PAX6 (ectoderm) was upregulated, compared with NC-treated samples on the 5PM surface (Figure 6G). Additionally, identical outcomes in the hESC cell line (Figure 6H) demonstrated that the universal promoting effects of BCCs on cardiogenesis were via the activity of SETDB1.

Previously, loss of SETDB1 in the embryonic stage was reported to impair the mesoderm[42] and endoderm development.[43] However, the hiPSCs maintain low levels of H3K9me3, allowing the expressions of transcriptional regulators of neuronal differentiation. The Huntingtin disease-specific hiPSCs were reported to exhibit increased H3K9me3 levels, impairing the induction of distinct neural genes.[44] Consistently, the knockdown of SETDB1 downregulated the differentiation of hiPSCs into the mesoderm and endoderm lineages but upregulated the expressions of ectoderm markers in the present study.

CONCLUSION

The present study explored the mechanism of binary colloidal crystal (BCC)-induced mechanotransduction in the cardiac differentiation of hiPSCs, which is illustrated in the Table of Contents graphic. hiPSCs were more spherical and had a stiffer nucleus on the 5PM surface, accompanied by the down-regulation of the chromatin accessibility and promotion of the translocation of SETDB1 into the cell nucleus. hESCs showed similar behaviors, indicating that this phenomenon could be universal in pluripotent stem cells. It was demonstrated that the BCC substrate delivered the specific outside-in signals, which remodeled the chromatin state and in turn influenced the ultimate cell fate. This study provides insights into biophysics, materiobiology, and stem cell bioengineering.

METHODS

Fabrication of BCCs. BCCs were fabricated according to our previous protocol using evaporation-induced confined area assembly (EICAA).[45] Briefly, large silica (Si) particles and small polymer (polystyrene (PS) or poly(methyl methacrylate) (PMMA) particles were well-mixed in Milli-Q water and deposited on PS-coated glass slides in a confined area (i.e., a 3 cm diameter rubber ring). Four combinations were designed, 2 μm Si/0.1 μm PS (2PS), 2 μm Si/0.1 PMMA (2PM), 5 μm Si/0.4 PS (5PS), and 5 μm Si/0.4 μm PMMA (5PM) in this study. The volumes of the two colloidal solutions were calculated based on the concentration of large Si particles needed to form a monolayer inside the confined area. Polymer particles were calculated to fill the voids between Si particles without covering them. After water evaporation, the BCCs were heated to 200 °C for 1 min to stabilize the particle layers. BCCs were sterilized under UV light (ProCleaner Plus, BioForce Nanosciences, Inc.) for 30 min prior to cell culture.

X-ray Photoelectron Spectroscopy (XPS). Monochromated Alkα X-ray source with 150 W of power was used for the XPS analysis with a Kratos AXIS NOVA spectrometer (Kratos Analytical Inc., Manchester, UK).[46] The pass energies used to acquire the survey and high-resolution spectra were 160 and 20 eV, respectively. Three spots with elliptical areas of $\approx 0.3 \times 0.7$ mm^2 on each surface were analyzed. The CasaXPS processing software (version 2.3.16, Casa Software Ltd. Teignmouth, UK) was used to analyze and quantify the obtained data. All XPS spectra were corrected according to the C ls line at 284.6 eV.

Teratoma Formation and Karyotyping. Teratoma formation was performed to evaluate differentiation potency. 10^6 iPSCs in total were collected, resuspended in 100 μL of Matrigel, and transplanted to immune-deficient mice (NOD/SCID) of 6-week subcutaneously. Eight weeks later, teratomas were surgically dissected and fixed. Representative sections of hematoxylin and eosin (H&E) stain of all three germ layers were demonstrated.

For karyotyping analysis, colcemid (10 ug/mL) was used to treat iPSCs at 37 °C for 1 h. After being dissociated by Accutase (STEMCELL Technologies, #07920), iPSCs were collected, treated by hypotonic KCl solution at the concentration of 0.075 M at 37 °C for 20 min, and fixed by Carnoy's fixative. Next, Giemsa stain was performed. Twenty cells in metaphase were counted for G-banding analysis.

Cell Culture and Differentiation. hiPSCs (NC5) and hESCs (H9) were cultured in mTeSR1 medium (STEMCELL Technologies, #85850) on matrigel (Corning, #354248) coated cell culture plates (Corning, #3506). hiPSCs and hESCs were maintained between passages 20 and 80, and passaged at 85−100% density with Accutase (STEMCELL Technologies, #07920) every 3−5 days. The protocol of cardiac differentiation was described before.[47] After 30 days of *in vitro* differentiation, the cells were trypsinized and reseeded on gelatin-coated coverslips for further experiments.

On the early days of the cardiogenesis, 100 nM JIB-04 (MCE, HY-13953) or 1 μM BIX-01294 (MCE, HY-10587) was added from D0 for 48 h to modulate the activity of SETDB1.

EB-Derived Cardiomyocytes. When the stem cells grow to 80% confluence, cells were digested with accutase for 3−5 min to dissociate colonies to single cells. To form self-aggregated EBs, suspending cells were transferred to the low attachment 6-well plate (Corning, # 3471), with 2 mL per well in the concentration of 5×10^6/mL. On the second day, EBs could form in various sizes and were maintained in the ED Formation Medium (AggreWell, # 05893) as reported before.[48]

On Day 4 since EB formation, cardiac differentiation was induced using small molecules as applied in monolayer differentiation. On Day 8 since cardiac differentiation, spontaneously beating cardiomyocytes could be observed and were fed every alternate day with the F12 Medium (Thermo Fisher, 11320033) + 2% FBS (Thermo Fisher,

https://doi.org/10.1021/acsnano.3c00009
ACS Nano 2023, 17, 3181−3193

10100147). During the whole process, culture dishes or plates were placed on the decolorization shaker (60 rpm) in a 37 °C incubator. After 30 days of *in vitro* differentiation, the cells were centrifugated (200g, 5 min), trypsinized, and reseeded on gelatin-coated coverslips for further experiments.

Three Germ Layer Differentiation Assay. A STEMdiff Trilineage Differentiation Kit (Stemcell Technologies, #130115660) was used for iPSCs differentiation *in vitro* following the manufacturer's protocol. Differentiated cells were analyzed with related markers for the endoderm, mesoderm, and ectoderm.

Atomic Force Microscope (AFM) Measurement. Cell stiffness was measured *in situ* using peak force tapping mode BioScope Resolve AFM (Bruker Corp., USA), and probes with spring constants of 0.061 N/m (MLCT-A, Bruker Corp., USA) were used. During the measurement, the cell activity was ensured by constant temperature perfusion of culture medium at 37 °C, the AFM tip was positioned on the top of the cell nucleus with micrometer precision, and force−displacement curves were recorded at 0.25 kHz. Hertz's model for mechanics was employed to analyze Young's modulus of cardiomyocytes. For the stiffness of BCCs, the materials were fixed on a Petri dish filled with PBS, force curves were directly collected in PBS using a cantilever with a calibrated spring constant, 0.802 N/m (NP-S10-A). All values of Young's modulus were obtained by Nasoscope Analysis 1.7 software (Bruker Corp., USA).

Scanning Electron Microscopy (SEM). The samples were washed with Dulbecco's phosphate-buffered saline (DPBS) and fixed with 2% cooled glutaraldehyde for 3 h. Samples were coated with a thin layer of gold for 10 s. A thermal field emission scanning electron microscopy (FE-SEM, JEOL JSM-7900F, Japan) was used to observe the samples.

Transmission Electron Microscope (TEM). The samples were placed in 2% cooled glutaraldehyde and fixed for 24 h. After fixation, the sample was treated with 1% osmic acid at room temperature for 7 h. Then samples were dehydrated with increasing concentrations of ethanol (50−100%, each concentration for 30 min). After embedding with EPON812, polymerization in a 60 °C oven, and block trimming, the samples were sliced into a thickness of 60−80 nm using an ultrathin slicer (Leica, Leica UC7, Germany). Slices were placed on a copper mesh, dried in 2% uranium acetate for 8 min, washed with deionized water, and then dyed in 2.6% lead citrate solution for 8 min. The images were collected and analyzed under a transmission electron microscope (JEOL, JEM-1010, Japan).

qRT-PCR. Total RNA was extracted using the TRIzol Reagent (Thermo Fisher Scientific, #15596026). The RNA was reverse-transcribed into cDNA using the PrimeScript RT Reagent kit (Takara, #RR037A) according to the manufacturer's instructions. For the qRT-PCR analysis, cDNA was amplified using an SYBR Green PCR Kit (Bio-Rad, #1725121). GAPDH was used as the housekeeping gene. In each group, three samples were analyzed. The detailed information on primers is listed in Table S4.

Western Blot. Total, cytoplasmic, and nuclear proteins were extracted from cells using a protein extraction kit (KeyGen BioTECH, KGP250, KGBSP002). Lysate protein concentrations were determined using the BCA method (Thermo Fisher Scientific, #23225). Protein extracts were transferred to a polyvinylidene difluoride (PVDF) membrane and blocked with 5% bovine serum albumin for nonspecific bindings. Then membranes were incubated overnight at 4 °C with primary antibodies, followed by incubation with Horseradish Peroxidase conjugated secondary antibodies. Images were captured using a Western blot intelligent imaging system (iBrigh CL1000, Thermo Fisher Scientific, Singapore) and analyzed using ImageJ software. The detailed information on antibodies is listed in Table S5.

Immunofluorescence Staining. Except for reseeded cardiomyocytes, hiPSCs on different surfaces were stained *in situ*. Briefly, cells were carefully washed three times using PBS and then fixed with 4% paraformaldehyde for 30 min, incubated with 0.1% Triton X-100/PBS for 10 min. Then the samples were blocked with 1% BSA at room temperature for 30 min. The samples were incubated with the primary antibody. After labeling with secondary antibody, cells were imaged using a Zeiss fluorescence microscope (Axio Imager A2, Zeiss, Germany) and analyzed using ImageJ software. The detailed information on antibodies is listed in Table S5.

ATAC-seq. First, we prepared cell suspension, lysed cells with lysate to obtain nuclei, then cut and purified them with Tn5 transposase, and finally recovered DNA fragments. The recovered fragments were subjected to end repair, 3′-end addition of A, the connection of sequencing connector, fragment size selection, and PCR amplification to obtain a standard high-throughput sequencing library. Sequencing was performed using an Illumina sequencing platform.[49] The original reads obtained by ATAC-seq were filtered to obtain clean reads. We obtained the peak position after comparing clean reads with the reference genome sequence. We mainly chose MACS2 v2 1.1 software for peak extraction.[50] Next, the associated genes in the peak region were compared with NR, Swiss-prot,[51] GO,[52] KEGG,[53] COG,[54] KOG,[55] eggNOG,[56] and Pfam[56] function database through BLAST[57] to obtain the annotation of these genes. Finally, the functional enrichment analysis was performed.

Statistical Analysis. All normally distributed data were represented as mean ± standard error of the mean, and the Student's *t* test was used to evaluate statistical significance between the two groups. Three or more groups were compared by one-way analysis of variance (ANOVA). A *p*-value less than 0.05 was considered statistically significant.

ASSOCIATED CONTENT

Supporting Information

The Supporting Information is available free of charge at https://pubs.acs.org/doi/10.1021/acsnano.3c00009.

Characteristics of BCC surfaces; teratoma assay and karyotype analysis of hiPSCs; hiPSC-CMs derived via EB formation; the gene expressions of distinct integrin subtypes; fluorescence staining of cytomembrane and cTnT in hiPSCs cultured on 5PM and control coverslips; immunofluorescence staining of endoderm and ectoderm markers; chromatin accessibility analysis of hiPSCs cultured on different surfaces; the representative genome tracks of ATAC-Seq reads in hiPSCs cultured on 5PM and control surfaces; the content of H3K4me3, H3K27me3, and H3K9me2 protein levels in hiPSCs on 5PM and control coverslips; young's modulus of control coverslip, 2PM, and 5PM with and without Matrigel coating; bright filed of hiPSCs cultured on control, 2PM, 5PM, and 5PM+Y-27632 treatment; immunostaining of hESC-CMs derived from control and 5PM surface; the number of the differentially accessible region (DARs); list of top 5 differentially expressed genes involved in multiple processes; siRNA sequence; primers sequence; detailed information on antibodies (PDF)

AUTHOR INFORMATION

Corresponding Authors

Minglong Chen − *Department of Cardiology, The First Affiliated Hospital of Nanjing Medical University, Nanjing 210000 Jiangsu, China; Department of Cardiology, The Affiliated Taizhou People's Hospital of Nanjing Medical University, Taizhou School of Clinical Medicine, Nanjing Medical University, Taizhou 225300 Jiangsu, China; Key Laboratory of Targeted Intervention of Cardiovascular Disease, Collaborative Innovation Center for Cardiovascular Disease Translational Medicine, Nanjing Medical University, Nanjing 210000 Jiangsu, China;* orcid.org/0000-0002-9844-486X; Email: chenminglong@njmu.edu.cn

https://doi.org/10.1021/acsnano.3c00009
ACS Nano 2023, 17, 3181−3193

Peng-Yuan Wang − *Oujiang Laboratory; Key Laboratory of Alzheimer's Disease of Zhejiang Province, Institute of Aging, Wenzhou Medical University, Wenzhou 325000 Zhejiang, China;* orcid.org/0000-0001-7965-2914; Email: py.wang@ojlab.ac.cn

Chang Cui − *Department of Cardiology, The First Affiliated Hospital of Nanjing Medical University, Nanjing 210000 Jiangsu, China;* orcid.org/0000-0002-5349-6295; Email: cuichang@njmu.edu.cn

Authors

Yongping Lin − *Department of Cardiology, The First Affiliated Hospital of Nanjing Medical University, Nanjing 210000 Jiangsu, China; Department of Cardiology, The Affiliated Taizhou People's Hospital of Nanjing Medical University, Taizhou School of Clinical Medicine, Nanjing Medical University, Taizhou 225300 Jiangsu, China*

Feng Zhang − *Department of Cardiology, The First Affiliated Hospital of Nanjing Medical University, Nanjing 210000 Jiangsu, China*

Shaojie Chen − *Department of Cardiology, The First Affiliated Hospital of Nanjing Medical University, Nanjing 210000 Jiangsu, China*

Xiyu Zhu − *Department of Cardio-Thoracic Surgery, Nanjing Drum Tower Hospital, The Affiliated Hospital of Nanjing University Medical School, Nanjing 210000, China*

Jincheng Jiao − *State Key Laboratory of Bioelectronics, School of Biological Science and Medical Engineering, Southeast University, Nanjing 210000 Jiangsu, China*

Yike Zhang − *Department of Cardiology, The First Affiliated Hospital of Nanjing Medical University, Nanjing 210000 Jiangsu, China*

Zhaomin Li − *Department of Cardiology, The First Affiliated Hospital of Nanjing Medical University, Nanjing 210000 Jiangsu, China*

Jiao Lin − *Shenzhen Key Laboratory of Biomimetic Materials and Cellular Immunomodulation, Shenzhen Institute of Advanced Technology, Chinese Academy of Sciences, Shenzhen 518000 Guangdong, China*

Biao Ma − *State Key Laboratory of Bioelectronics, School of Biological Science and Medical Engineering, Southeast University, Nanjing 210000 Jiangsu, China*

Complete contact information is available at: https://pubs.acs.org/10.1021/acsnano.3c00009

Author Contributions

#Y.L., F.Z., and S.C. contributed equally to this work. C.C., P.Y.W., and M.C. are listed as the cocorresponding authors, considering their significant contributions. C.C. designed and supervised the study. P.Y.W. and M.C. led the projects. Y.L., F.Z., and S.C. collected and assembled the data and wrote the manuscript. J.J., X.Z., Y.Z., and Z.L. collected and assembled data. J.L. and B.M. provided the material. All authors revised and agree to publish the manuscript.

Funding

The research was funded by the National Natural and Science Foundation of China (Grant No. 81900295 to C. Cui, 82200352 to F. Zhang, 31870988 to P. Wang, and 82070343 to M. Chen), Natural Science Foundation of Jiangsu Province of China (Grant No. BK20191071 to C. Cui and BK20220710 to F. Zhang), the Ministry of Science and Technology of China (2022YFA1105101 to P. Y. Wang), Zhejiang Provincial Natural Science Foundation of China (LZ23C070004 to P. Y. Wang); the Chinese Academy of Sciences (172644KYSB20200002 and 172644KYSB20200048 to P. Y. Wang), the Department of Science and Technology of Guangdong Province (2021A0505030055 to P. Y. Wang), and the Science, Technology, and Innovation Commission of Shenzhen Municipality (GJHZ20180928115804736 and ZDSYS20190902093409851 to P. Y. Wang).

Notes

The authors declare no competing financial interest.

REFERENCES

(1) Devalla, H. D.; Passier, R., Cardiac differentiation of pluripotent stem cells and implications for modeling the heart in health and disease. *Sci. Transl Med.***2018**, *10* (435). DOI: 10.1126/scitranslmed.aah5457

(2) Hwang, N. S.; Varghese, S.; Elisseeff, J. Controlled differentiation of stem cells. *Adv. Drug Deliv Rev.* **2008**, *60* (2), 199−214.

(3) Killaars, A. R.; Grim, J. C.; Walker, C. J.; Hushka, E. A.; Brown, T. E.; Anseth, K. S. Extended Exposure to Stiff Microenvironments Leads to Persistent Chromatin Remodeling in Human Mesenchymal Stem Cells. *Adv. Sci. (Weinh)* **2019**, *6* (3), 1801483.

(4) McBeath, R.; Pirone, D. M.; Nelson, C. M.; Bhadriraju, K.; Chen, C. S. Cell shape, cytoskeletal tension, and RhoA regulate stem cell lineage commitment. *Dev Cell* **2004**, *6* (4), 483−95.

(5) Seelbinder, B.; Ghosh, S.; Schneider, S. E.; Scott, A. K.; Berman, A. G.; Goergen, C. J.; Margulies, K. B.; Bedi, K. C., Jr; Casas, E.; Swearingen, A. R.; Brumbaugh, J.; Calve, S.; Neu, C. P. Nuclear deformation guides chromatin reorganization in cardiac development and disease. *Nat. Biomed Eng.* **2021**, *5* (12), 1500−1516.

(6) Ayuningtyas, F. D.; Kim, M. H.; Kino-Oka, M. Muscle lineage switching by migratory behaviour-driven epigenetic modifications of human mesenchymal stem cells on a dendrimer-immobilized surface. *Acta Biomater* **2020**, *106*, 170−180.

(7) Morez, C.; Noseda, M.; Paiva, M. A.; Belian, E.; Schneider, M. D.; Stevens, M. M. Enhanced efficiency of genetic programming toward cardiomyocyte creation through topographical cues. *Biomaterials* **2015**, *70*, 94−104.

(8) Cui, C.; Wang, J.; Qian, D.; Huang, J.; Lin, J.; Kingshott, P.; Wang, P. Y.; Chen, M. Binary Colloidal Crystals Drive Spheroid Formation and Accelerate Maturation of Human-Induced Pluripotent Stem Cell-Derived Cardiomyocytes. *ACS Appl. Mater. Interfaces* **2019**, *11* (4), 3679−3689.

(9) Diba, F.; Reynolds, N.; Thissen, H.; Wang, P.-Y.; Kingshott, P. Tunable Chemical and Topographic Patterns Based on Binary Colloidal Crystals (BCCs) to Modulate MG63 Cell Growth. *Adv. Funct. Mater.* **2019**, *29*, 1904262.

(10) Barzegari, A.; Omidi, Y.; Ostadrahimi, A.; Gueguen, V.; Meddahi-Pellé, A.; Nouri, M.; Pavon-Djavid, G. The role of Piezo proteins and cellular mechanosensing in tuning the fate of transplanted stem cells. *Cell Tissue Res.* **2020**, *381* (1), 1−12.

(11) Eichholz, K. F.; Woods, I.; Riffault, M.; Johnson, G. P.; Corrigan, M.; Lowry, M. C.; Shen, N.; Labour, M. N.; Wynne, K.; O'Driscoll, L.; Hoey, D. A. Human bone marrow stem/stromal cell osteogenesis is regulated via mechanically activated osteocyte-derived extracellular vesicles. *Stem Cells Transl Med.* **2020**, *9* (11), 1431−1447.

(12) Wang, J.; Chen, A.; Lieu, D. K.; Karakikes, I.; Chen, G.; Keung, W.; Chan, C. W.; Hajjar, R. J.; Costa, K. D.; Khine, M.; Li, R. A. Effect of engineered anisotropy on the susceptibility of human pluripotent stem cell-derived ventricular cardiomyocytes to arrhythmias. *Biomaterials* **2013**, *34* (35), 8878−86.

(13) Kit-Anan, W.; Mazo, M. M.; Wang, B. X.; Leonardo, V.; Pence, I. J.; Gopal, S.; Gelmi, A.; Nagelkerke, A.; Becce, M.; Chiappini, C.; Harding, S. E.; Terracciano, C. M.; Stevens, M. M. Multiplexing physical stimulation on single human induced pluripotent stem cell-derived cardiomyocytes for phenotype modulation. *Biofabrication* **2021**, *13* (2), 025004.

(14) Goldfracht, I.; Efraim, Y.; Shinnawi, R.; Kovalev, E.; Huber, I.; Gepstein, A.; Arbel, G.; Shaheen, N.; Tiburcy, M.; Zimmermann, W. H.; Machluf, M.; Gepstein, L. Engineered heart tissue models from hiPSC-derived cardiomyocytes and cardiac ECM for disease modeling and drug testing applications. *Acta Biomater* **2019**, *92*, 145−159.
(15) Shi, Y.; Lin, J.; Tao, X.; Qu, J.; Liao, S.; Li, M.; Deng, K.; Du, P.; Liu, K.; Thissen, H.; Li, L.; Kingshott, P.; Wang, P. Y. Harnessing Colloidal Self-Assembled Patterns (cSAPs) to Regulate Bacterial and Human Stem Cell Response at Biointerfaces In Vitro and In Vivo. *ACS Appl. Mater. Interfaces* **2021**, *13* (18), 20982−20994.
(16) Kentish, J. C.; ter Keurs, H. E.; Ricciardi, L.; Bucx, J. J.; Noble, M. I. Comparison between the sarcomere length-force relations of intact and skinned trabeculae from rat right ventricle. Influence of calcium concentrations on these relations. *Circ. Res.* **1986**, *58* (6), 755−68.
(17) Versaevel, M.; Grevesse, T.; Gabriele, S. Spatial coordination between cell and nuclear shape within micropatterned endothelial cells. *Nat. Commun.* **2012**, *3*, 671.
(18) Wang, Z.; Oron, E.; Nelson, B.; Razis, S.; Ivanova, N. Distinct lineage specification roles for NANOG, OCT4, and SOX2 in human embryonic stem cells. *Cell Stem Cell* **2012**, *10* (4), 440−54.
(19) Bernardo, A. S.; Faial, T.; Gardner, L.; Niakan, K. K.; Ortmann, D.; Senner, C. E.; Callery, E. M.; Trotter, M. W.; Hemberger, M.; Smith, J. C.; Bardwell, L.; Moffett, A.; Pedersen, R. A. BRACHYURY and CDX2 mediate BMP-induced differentiation of human and mouse pluripotent stem cells into embryonic and extraembryonic lineages. *Cell Stem Cell* **2011**, *9* (2), 144−55.
(20) Zhang, L.; Nomura-Kitabayashi, A.; Sultana, N.; Cai, W.; Cai, X.; Moon, A. M.; Cai, C. L. Mesodermal Nkx2.5 is necessary and sufficient for early second heart field development. *Dev. Biol.* **2014**, *390* (1), 68−79.
(21) Romayor, I.; Herrera, L.; Burón, M.; Martin-Inaraja, M.; Prieto, L.; Etxaniz, J.; Inglés-Ferrándiz, M.; Pineda, J. R.; Eguizabal, C. A Comparative Study of Cell Culture Conditions during Conversion from Primed to Naive Human Pluripotent Stem Cells. *Biomedicines* **2022**, *10* (6), 1358.
(22) Maldonado, M.; Luu, R. J.; Ico, G.; Ospina, A.; Myung, D.; Shih, H. P.; Nam, J. Lineage- and developmental stage-specific mechanomodulation of induced pluripotent stem cell differentiation. *Stem Cell Res. Ther* **2017**, *8* (1), 216.
(23) Chalut, K. J.; Höpfler, M.; Lautenschläger, F.; Boyde, L.; Chan, C. J.; Ekpenyong, A.; Martinez-Arias, A.; Guck, J. Chromatin decondensation and nuclear softening accompany Nanog down-regulation in embryonic stem cells. *Biophys. J.* **2012**, *103* (10), 2060−70.
(24) Stephens, A. D.; Liu, P. Z.; Kandula, V.; Chen, H.; Almassalha, L. M.; Herman, C.; Backman, V.; O'Halloran, T.; Adam, S. A.; Goldman, R. D.; Banigan, E. J.; Marko, J. F. Physicochemical mechanotransduction alters nuclear shape and mechanics via heterochromatin formation. *Mol. Biol. Cell* **2019**, *30* (17), 2320−2330.
(25) Hofbauer, P.; Jahnel, S. M.; Papai, N.; Giesshammer, M.; Deyett, A.; Schmidt, C.; Penc, M.; Tavernini, K.; Grdseloff, N.; Meledeth, C.; Ginistrelli, L. C.; Ctortecka, C.; Šalic, Š.; Novatchkova, M.; Mendjan, S. Cardioids reveal self-organizing principles of human cardiogenesis. *Cell* **2021**, *184* (12), 3299−3317.e22.
(26) MacGrogan, D.; Münch, J.; de la Pompa, J. L. Notch and interacting signalling pathways in cardiac development, disease, and regeneration. *Nat. Rev. Cardiol* **2018**, *15* (11), 685−704.
(27) Artap, S.; Manderfield, L. J.; Smith, C. L.; Poleshko, A.; Aghajanian, H.; See, K.; Li, L.; Jain, R.; Epstein, J. A. Endocardial Hippo signaling regulates myocardial growth and cardiogenesis. *Dev. Biol.* **2018**, *440* (1), 22−30.
(28) Bylund, J. B.; Trinh, L. T.; Awgulewitsch, C. P.; Paik, D. T.; Jetter, C.; Jha, R.; Zhang, J.; Nolan, K.; Xu, C.; Thompson, T. B.; Kamp, T. J.; Hatzopoulos, A. K. Coordinated Proliferation and Differentiation of Human-Induced Pluripotent Stem Cell-Derived Cardiac Progenitor Cells Depend on Bone Morphogenetic Protein Signaling Regulation by GREMLIN 2. *Stem Cells Dev* **2017**, *26* (9), 678−693.
(29) Okuda, A.; Fukushima, A.; Nishimoto, M.; Orimo, A.; Yamagishi, T.; Nabeshima, Y.; Kuro-o, M.; Nabeshima, Y.; Boon, K.; Keaveney, M.; Stunnenberg, H. G.; Muramatsu, M. UTF1, a novel transcriptional coactivator expressed in pluripotent embryonic stem cells and extra-embryonic cells. *Embo j* **1998**, *17* (7), 2019−32.
(30) Peng, G.; Suo, S.; Cui, G.; Yu, F.; Wang, R.; Chen, J.; Chen, S.; Liu, Z.; Chen, G.; Qian, Y.; Tam, P. P. L.; Han, J. J.; Jing, N. Molecular architecture of lineage allocation and tissue organization in early mouse embryo. *Nature* **2019**, *572* (7770), 528−532.
(31) Carter, B.; Zhao, K. The epigenetic basis of cellular heterogeneity. *Nat. Rev. Genet* **2021**, *22* (4), 235−250.
(32) Strahl, B. D.; Allis, C. D. The language of covalent histone modifications. *Nature* **2000**, *403* (6765), 41−5.
(33) Beyer, S.; Pontis, J.; Schirwis, E.; Battisti, V.; Rudolf, A.; Le Grand, F.; Ait-Si-Ali, S. Canonical Wnt signalling regulates nuclear export of Setdb1 during skeletal muscle terminal differentiation. *Cell Discov* **2016**, *2*, 16037.
(34) Calvo, F.; Ege, N.; Grande-Garcia, A.; Hooper, S.; Jenkins, R. P.; Chaudhry, S. I.; Harrington, K.; Williamson, P.; Moeendarbary, E.; Charras, G.; Sahai, E. Mechanotransduction and YAP-dependent matrix remodelling is required for the generation and maintenance of cancer-associated fibroblasts. *Nat. Cell Biol.* **2013**, *15* (6), 637−46.
(35) Uehata, M.; Ishizaki, T.; Satoh, H.; Ono, T.; Kawahara, T.; Morishita, T.; Tamakawa, H.; Yamagami, K.; Inui, J.; Maekawa, M.; Narumiya, S. Calcium sensitization of smooth muscle mediated by a Rho-associated protein kinase in hypertension. *Nature* **1997**, *389* (6654), 990−4.
(36) Nava, M. M.; Miroshnikova, Y. A.; Biggs, L. C.; Whitefield, D. B.; Metge, F.; Boucas, J.; Vihinen, H.; Jokitalo, E.; Li, X.; García Arcos, J. M.; Hoffmann, B.; Merkel, R.; Niessen, C. M.; Dahl, K. N.; Wickström, S. A. Heterochromatin-Driven Nuclear Softening Protects the Genome against Mechanical Stress-Induced Damage. *Cell* **2020**, *181* (4), 800−817.e22.
(37) Zhao, X. B.; Chen, Y. P.; Tan, M.; Zhao, L.; Zhai, Y. Y.; Sun, Y. L.; Gong, Y.; Feng, X. Q.; Du, J.; Fan, Y. B. Extracellular Matrix Stiffness Regulates DNA Methylation by PKCα-Dependent Nuclear Transport of DNMT3L. *Adv. Healthc Mater.* **2021**, *10* (16), 2170076.
(38) Yuan, P.; Han, J.; Guo, G.; Orlov, Y. L.; Huss, M.; Loh, Y. H.; Yaw, L. P.; Robson, P.; Lim, B.; Ng, H. H. Eset partners with Oct4 to restrict extraembryonic trophoblast lineage potential in embryonic stem cells. *Genes Dev.* **2009**, *23* (21), 2507−20.
(39) Wu, K.; Liu, H.; Wang, Y.; He, J.; Xu, S.; Chen, Y.; Kuang, J.; Liu, J.; Guo, L.; Li, D.; Shi, R.; Shen, L.; Wang, Y.; Zhang, X.; Wang, J.; Pei, D.; Chen, J. SETDB1-Mediated Cell Fate Transition between 2C-Like and Pluripotent States. *Cell Rep* **2020**, *30* (1), 25−36.e6.
(40) Nicetto, D.; Donahue, G.; Jain, T.; Peng, T.; Sidoli, S.; Sheng, L.; Montavon, T.; Becker, J. S.; Grindheim, J. M.; Blahnik, K.; Garcia, B. A.; Tan, K.; Bonasio, R.; Jenuwein, T.; Zaret, K. S. H3K9me3-heterochromatin loss at protein-coding genes enables developmental lineage specification. *Science* **2019**, *363* (6424), 294−297.
(41) Song, Y.; Soto, J.; Chen, B.; Hoffman, T.; Zhao, W.; Zhu, N.; Peng, Q.; Liu, L.; Ly, C.; Wong, P. K.; Wang, Y.; Rowat, A. C.; Kurdistani, S. K.; Li, S. Transient nuclear deformation primes epigenetic state and promotes cell reprogramming. *Nat. Mater.* **2022**, *21* (10), 1191−1199.
(42) Mochizuki, K.; Tando, Y.; Sekinaka, T.; Otsuka, K.; Hayashi, Y.; Kobayashi, H.; Kamio, A.; Ito-Matsuoka, Y.; Takehara, A.; Kono, T.; Osumi, N.; Matsui, Y. SETDB1 is essential for mouse primordial germ cell fate determination by ensuring BMP signaling. *Development* **2018**, *145* (23), dev164160 DOI: 10.1242/dev.164160.
(43) Wang, Z.; Fan, R.; Russo, A.; Cernilogar, F. M.; Nuber, A.; Schirge, S.; Shcherbakova, I.; Dzhilyanova, I.; Ugur, E.; Anton, T.; Richter, L.; Leonhardt, H.; Lickert, H.; Schotta, G. Dominant role of DNA methylation over H3K9me3 for IAP silencing in endoderm. *Nat. Commun.* **2022**, *13* (1), 5447.
(44) Irmak, D.; Fatima, A.; Gutiérrez-Garcia, R.; Rinschen, M. M.; Wagle, P.; Altmüller, J.; Arrigoni, L.; Hummel, B.; Klein, C.; Frese, C.

K.; Sawarkar, R.; Rada-Iglesias, A.; Vilchez, D. Mechanism suppressing H3K9 trimethylation in pluripotent stem cells and its demise by polyQ-expanded huntingtin mutations. *Hum. Mol. Genet.* **2018**, *27* (23), 4117−4134.
(45) Wang, P. Y.; Thissen, H.; Kingshott, P. Stimulation of Early Osteochondral Differentiation of Human Mesenchymal Stem Cells Using Binary Colloidal Crystals (BCCs). *ACS Appl. Mater. Interfaces* **2016**, *8* (7), 4477−88.
(46) Pingle, H.; Wang, P. Y.; Thissen, H.; Kingshott, P. Controlled Attachment of Pseudomonas aeruginosa with Binary Colloidal Crystal-Based Topographies. *Small* **2018**, *14* (14), e1703574.
(47) Wang, J.; Cui, C.; Nan, H.; Yu, Y.; Xiao, Y.; Poon, E.; Yang, G.; Wang, X.; Wang, C.; Li, L.; Boheler, K. R.; Ma, X.; Cheng, X.; Ni, Z.; Chen, M. Graphene Sheet-Induced Global Maturation of Cardiomyocytes Derived from Human Induced Pluripotent Stem Cells. *ACS Appl. Mater. Interfaces* **2017**, *9* (31), 25929−25940.
(48) Lin, Y.; Chen, G., Embryoid body formation from human pluripotent stem cells in chemically defined E8 media. In *StemBook*; Yongshun, L., Guokai, C., Eds.; Harvard Stem Cell Institute: Cambridge, MA, 2008.
(49) Buenrostro, J. D.; Wu, B.; Chang, H. Y.; Greenleaf, W. J. ATAC-seq: A Method for Assaying Chromatin Accessibility Genome-Wide. *Curr. Protoc Mol. Biol.* **2015**, *109*, 21.29.1−21.29.9.
(50) Zhang, Y.; Liu, T.; Meyer, C. A.; Eeckhoute, J.; Johnson, D. S.; Bernstein, B. E.; Nusbaum, C.; Myers, R. M.; Brown, M.; Li, W.; Liu, X. S. Model-based analysis of ChIP-Seq (MACS). *Genome Biol.* **2008**, *9* (9), R137.
(51) Apweiler, R.; Bairoch, A.; Wu, C. H.; Barker, W. C.; Boeckmann, B.; Ferro, S.; Gasteiger, E.; Huang, H.; Lopez, R.; Magrane, M.; Martin, M. J.; Natale, D. A.; O'Donovan, C.; Redaschi, N.; Yeh, L. S. UniProt: the Universal Protein knowledgebase. *Nucleic Acids Res.* **2004**, *32* (Databaseissue), D115−9.
(52) Ashburner, M.; Ball, C. A.; Blake, J. A.; Botstein, D.; Butler, H.; Cherry, J. M.; Davis, A. P.; Dolinski, K.; Dwight, S. S.; Eppig, J. T.; Harris, M. A.; Hill, D. P.; Issel-Tarver, L.; Kasarskis, A.; Lewis, S.; Matese, J. C.; Richardson, J. E.; Ringwald, M.; Rubin, G. M.; Sherlock, G. Gene ontology: tool for the unification of biology. The Gene Ontology Consortium. *Nat. Genet.* **2000**, *25* (1), 25−9.
(53) Kanehisa, M.; Goto, S.; Kawashima, S.; Okuno, Y.; Hattori, M. The KEGG resource for deciphering the genome. *Nucleic Acids Res.* **2004**, *32* (Database issue), D277−80.
(54) Tatusov, R. L.; Galperin, M. Y.; Natale, D. A.; Koonin, E. V. The COG database: a tool for genome-scale analysis of protein functions and evolution. *Nucleic Acids Res.* **2000**, *28* (1), 33−6.
(55) Koonin, E. V.; Fedorova, N. D.; Jackson, J. D.; Jacobs, A. R.; Krylov, D. M.; Makarova, K. S.; Mazumder, R.; Mekhedov, S. L.; Nikolskaya, A. N.; Rao, B. S.; Rogozin, I. B.; Smirnov, S.; Sorokin, A. V.; Sverdlov, A. V.; Vasudevan, S.; Wolf, Y. I.; Yin, J. J.; Natale, D. A. A comprehensive evolutionary classification of proteins encoded in complete eukaryotic genomes. *Genome Biol.* **2004**, *5* (2), R7.
(56) Huerta-Cepas, J.; Szklarczyk, D.; Forslund, K.; Cook, H.; Heller, D.; Walter, M. C.; Rattei, T.; Mende, D. R.; Sunagawa, S.; Kuhn, M.; Jensen, L. J.; von Mering, C.; Bork, P. eggNOG 4.5: a hierarchical orthology framework with improved functional annotations for eukaryotic, prokaryotic and viral sequences. *Nucleic Acids Res.* **2016**, *44* (D1), D286−93.
(57) Altschul, S. F.; Madden, T. L.; Schäffer, A. A.; Zhang, J.; Zhang, Z.; Miller, W.; Lipman, D. J. Gapped BLAST and PSI-BLAST: a new generation of protein database search programs. *Nucleic Acids Res.* **1997**, *25* (17), 3389−402.

https://doi.org/10.1021/acsnano.3c00009
ACS Nano 2023, 17, 3181−3193